J-Researchers

Journal of Civil Engineering Researchers

Journal homepage: www.journals-researchers.com

Forensic Investigation and Petrographic Analysis of Concrete Apron Distresses; A Case Study in Nashville, Tennesse)

Hossein Alimohammadi,[a,*] David A. Been,[a] and James Duncan[a]

[a] *Terracon Consultants, Inc., Nashville, TN, USA 37217*

ABSTRACT

This study presents a forensic investigation into pavement distress in a concrete apron located in Nashville, Tennessee. The investigation involved detailed engineering observations and a comprehensive pavement condition survey in accordance with ASTM D5340. To identify the underlying causes of deterioration, petrographic examinations were conducted on three concrete cores extracted from the apron, following ASTM C856 guidelines. The analysis revealed consistent aggregate distribution, primarily composed of micritic limestone and quartz-based sand, with air content (total of entrapped and purposefully entrained air) ranging from 3.9% to 5.2% and air void spacing factors exceeding American Concrete Institute (ACI) recommendations for freeze-thaw durability. No carbonation was detected in the cores, but moderate to abundant ettringite, calcium hydroxide, and alkali-silica gel resulting from Alkali-Silica Gel (ASG) were observed lining voids and fractures. The findings indicate that Alkali-Silica Reaction (ASR)-related damage, exacerbated by cyclic wetting and drying, is a primary contributor to the pavement deterioration. Freeze-thaw damage due to inadequate air entrainment was also identified as a contributing factor. Based on the results, recommendations for improving the long-term performance and durability of the concrete apron include using low-alkali cement, selecting better-graded and less reactive aggregates, increasing the percentage of purposefully entrained air to reduce air void spacing and improve freeze-thaw durability, and incorporating supplementary cementitious materials (SCMs) to reduce alkali availability and enhance ASR resistance. We note the use of lithium nitrate has also been proven to mitigate ASR in new concrete. However, the mechanism of mitigation is not fully understood, and the relatively high cost and limited availability of lithium introduces challenges for this alternative. This study underscores the importance of petrographic examination in understanding concrete deterioration mechanisms and developing targeted repair strategies to enhance infrastructure durability.

ARTICLE INFO

Received: April 05, 2025
Accepted: August 21, 2025

Keywords:
Concrete Apron
Petrographic Examination
Freeze-thaw Damage
Freeze-thaw Damage
Petrographic Analysis

DOI: 10.61186/JCER.7.3.40
DOR: 20.1001.1.2538516.2025.7.3.4.4

1. Introduction

Concrete pavements are widely used in infrastructure due to their strength, durability, and cost-effectiveness. Their ability to withstand heavy loads and environmental stresses makes them a preferred choice for highways, airport runways and aprons, and other critical infrastructure [1] to [3]. However, despite their inherent strength,

* Corresponding author. Tel.: +12254853307; e-mail: Hossein.Alimohammadi@terracon.com.

concrete pavements are susceptible to various forms of deterioration over time, including cracking, scaling, and spalling, which can significantly reduce their lifespan and structural integrity. Among the various mechanisms of concrete deterioration, alkali-silica reaction (ASR) is one of the most critical factors affecting the long-term durability of concrete pavements. ASR leads to the formation of expansive gels within the concrete matrix, causing internal stresses that result in cracking and surface degradation. Understanding the causes and progression of ASR is essential for improving the performance and longevity of concrete pavements [4] to [8].

Petrographic analysis has emerged as a valuable tool for diagnosing the causes of concrete deterioration, including ASR and other chemical and physical damage. It provides critical insights into the microstructural and mineralogical characteristics of concrete, enabling engineers to identify reactive aggregates, monitor gel formation, and assess microcracking [9] to [15]. The ability to diagnose ASR-related distress at an early stage allows for the implementation of targeted mitigation strategies, improving the performance and longevity of concrete pavements. Petrography involves the microscopic examination of concrete core samples to evaluate the composition, texture, and microstructural characteristics of concrete. The American Society for Testing and Materials (ASTM) provides guidelines for petrographic examination under ASTM C856 – Standard Practice for Petrographic Examination of Hardened Concrete (ASTM, 2022) [1]. Petrographic analysis helps identify the mineralogical composition of aggregates, the presence of reactive products, microcracking patterns, and evidence of chemical reactions such as ASR. Through petrography, engineers can diagnose deterioration mechanisms, evaluate the quality of construction materials, and assess the effectiveness of mitigation strategies [16] to [22].

Alkali-silica reaction is a chemical reaction between the hydroxyl ions (OH^-) in the pore solution of concrete and reactive silica in aggregates. When reactive aggregates, such as opaline chert, strained quartz, and volcanic glass, are exposed to high-alkali environments, they form an expansive alkali-silica gel. This gel absorbs moisture and swells, generating internal tensile stresses that lead to cracking, surface spalling, and reduced structural integrity of concrete pavements (Swamy, 2002) [23] to [29]. The severity of ASR-related damage depends on several factors, including the type and reactivity of aggregates, the alkali content of the cement, and the availability of moisture (Thomas et al., 2013). Fournier and Bérubé (2000) [30] demonstrated that ASR-related damage is progressive and accelerates under cyclic wetting and drying conditions, which increase moisture availability and enhance the swelling of the gel.

Petrographic analysis allows for the early detection of ASR-related distress by identifying reactive products and microstructural changes in concrete. ASR gel typically appears as a birefringent material under polarized light microscopy, forming within cracks and voids around reactive aggregates. The formation of microcracks and reaction rims on aggregate surfaces is a common indicator of ASR activity (Thomas and Fournier, 2013) [31]. Optical microscopy is used to identify aggregate types, cracks, and reaction products, while scanning electron microscopy (SEM) provides detailed insights into the chemical composition and morphology of the gel (Scrivener & Kirkpatrick, 2008). SEM combined with energy-dispersive spectroscopy (EDS) allows for precise identification of reaction phases and the extent of silica dissolution [32] to [37].

Petrographic examination is instrumental in diagnosing ASR and assessing its impact on concrete durability. It enables the identification of reactive aggregates, the degree of microcracking, and the distribution of alkali-silica gel within the concrete matrix. Poole (1991) [38] emphasized that petrographic analysis provides a detailed understanding of the microstructure of concrete and the interaction between aggregates and the cement paste. This information is critical for identifying the root causes of ASR and implementing effective mitigation strategies.

Studies have shown that ASR-related damage is influenced by both intrinsic and extrinsic factors. Intrinsic factors include the mineralogical composition of aggregates and the chemical properties of the cement. Aggregates containing opal, chert, and strained quartz are highly susceptible to ASR due to their high silica content and reactive nature (Stark, 1991) [39]. The alkali content of the cement also plays a significant role, with high-alkali cements increasing the availability of hydroxyl ions for the reaction. Extrinsic factors such as moisture availability, temperature fluctuations, and exposure to deicing salts further accelerate ASR-related deterioration (Sanchez et al., 2017). Pavements subjected to high traffic loading experience additional mechanical stresses that exacerbate internal cracking, moisture infiltration and the progression of ASR (Stark and Gress, 1994) [40].

Petrographic analysis also has proven useful in evaluating the effectiveness of mitigation strategies for ASR. The use of supplementary cementitious materials (SCMs) such as fly ash, slag, and silica fume has been shown to reduce ASR by lowering the alkali content of the concrete and modifying the pore structure (Shehata and Thomas, 2000) [41]. SCMs reduce the availability of hydroxyl ions and limit the expansion of alkali-silica gel, thereby improving the durability of concrete pavements. Petrographic examination of SCM-treated concrete often reveals reduced gel formation, improved aggregate-paste

bonding, and decreased microcracking, confirming the success of these mitigation strategies.

Petrographic analysis provides insights into secondary reactions and microstructural changes associated with ASR. The formation of secondary deposits, such as calcium hydroxide and ettringite, within cracks and voids is a sign of ongoing chemical activity (Grattan-Bellew, 1995) [42]. Delayed ettringite formation (DEF) is another durability issue that can occur in conjunction with ASR, particularly in high-temperature curing conditions. DEF leads to additional expansion and cracking, compounding the damage caused by ASR (Taylor, 1997) [43]. The identification of these secondary products through petrography provides valuable evidence of the chemical and physical processes affecting concrete performance.

Microstructural defects such as poor compaction, inadequate air-void spacing, and improper aggregate grading can also compromise concrete durability [44] to [51]. Petrographic examination helps identify these flaws and their contribution to reduced performance. Mehta and Monteiro (2014) [52] noted that well-graded aggregates, low water-cement ratios, and proper curing enhance concrete durability, while deficiencies in these areas lead to increased permeability, shrinkage cracking, and freeze-thaw damage. Petrography provides a means of diagnosing these issues and informing corrective measures [53] to [62].

a) b)

Figure 1 a) and b) existing durability cracking and potential alkali-silica reaction distresses observed on the existing concrete

This study includes a forensic investigation of concrete pavement distress in Tennessee, focusing on ASR-related damage in a concrete apron. Concrete core samples were extracted and analyzed using petrographic techniques to identify the presence of reactive aggregates, alkali-silica gel, and microcracking patterns. The analysis provided evidence of ASR activity and highlighted contributing factors such as high alkali content in the cement, aggregate reactivity, exposure to moisture, lack of purposefully entrained air and excessive air void spacing. Based on the findings, recommendations were developed for mitigating ASR and improving the long-term performance of the concrete apron. These recommendations included the use of low-alkali cement, improved aggregate selection, the incorporation of SCMs to reduce alkali availability and improve resistance to ASR and increasing the amount of purposefully entrained air to improve freeze-thaw durability. The findings from this study highlight the importance of petrographic examination in forensic investigations and the development of durable concrete mixtures. Further advancements in petrographic techniques and analytical methods will continue to enhance the understanding and management of ASR and other durability challenges in concrete infrastructure.

2. Case study information, introduction and background

This study was conducted first to evaluate the Pavement Condition Index (PCI) of an existing concrete apron located in Nashville, Tennessee. The primary objective was to perform a forensic investigation of the existing distresses observed in the concrete apron and to provide recommendations for addressing the underlying causes and developing an appropriate rehabilitation plan. Terracon performed detailed engineering observations and a comprehensive condition survey during site visits. The surveyed area covered approximately 100,003 square feet of concrete apron. A range of distresses of varying severity levels were identified on the concrete apron during the survey. The observed distress types included: Corner Breaks, Settlement/Faulting, Longitudinal, Transverse, and Diagonal Cracks, Joint Seal Damage, Spalling at Corners and Joints, Patching (Small, $\leq$ 5 square feet), Scaling, Durability Cracking (D-Cracking), and evidence of Alkali-Silica Reaction (ASR). The visual pavement condition survey was conducted in general accordance with ASTM D5340 and locally accepted pavement engineering practices. Evidence of durability cracking, slab division, corner breaks, and joint spalling was present in all sample unit slabs of the rigid concrete pavement apron. These types of failures are typically associated with factors such as Freeze-thaw susceptibility of the aggregates, Poor concrete quality, Chemical reactions between the aggregates and the cementitious matrix, Over-finishing of the slab, Loss of surface moisture during placement due to environmental conditions (e.g., air temperature and wind).

The D-cracking observed at the joints of the concrete panels indicated a significant issue with freeze-thaw durability of the concrete and exposure to moisture. The widespread map cracking in the concrete apron slabs, extrusion of joint sealant and spalling of the concrete suggested the potential involvement of alkali-silica reaction (ASR). To confirm the presence of ASR and better understand the distress mechanisms, a petrographic investigation involving core sampling was performed. This testing enabled a more accurate diagnosis of the underlying causes and allowed for the formulation of targeted repair solutions. Figures 1 a and b illustrate the existing durability

cracking and alkali-silica reaction distresses observed on the existing concrete.

3. Petrographic Examinations

Three concrete cores (designated as C-1 through C-3), each with a diameter of 95 mm, were extracted from the site and analyzed at Terracon's materials laboratory in Cincinnati, Ohio. The objective of the petrographic examination was to identify the cause(s) of the observed cracking and deterioration. The investigation was performed in accordance with ASTM C856. As restrictions to this study, it should be mentioned that no approved concrete mix design, batch plant records, or concrete break reports (beams and/or cylinders) were available for review. Additionally, daily field observation reports containing information regarding ambient weather conditions during placement, construction procedures, or finishing methods were not provided. Lack of pertinent information is unfortunately typical in forensic/failure studies. Therefore, all findings and conclusions are based exclusively on the observations from the obtained cores.

Table 1
Concrete Proportions and Hardened Air Contents, % Volume

Core ID	Total Aggregate	Total Hardened Paste[1]	Total Air[2]
C1	61.7	33.1	5.2 (1.6)
C2	65.2	30.2	4.6 (2.4)
C3	65.3	30.8	3.9 (2.3)

1- Hardened paste includes the total of all cementitious materials.
2- Numbers in parentheses represent entrapped-size air (>0.04 inches). ASTM C457 (procedure B) does not distinguish between entrained and entrapped air. The distinction is made by the petrographer based on void size, shape, and location.

Table 2
Air Void System Parameters

Core ID	Length of Traverse (in)	Total Air Content (%)	Paste/Air Ratio[1]	Void Frequency (voids/mm)[2]	Average Chord Length (mm)	Specific Surface (mm^2/mm^3)[2]	Void Spacing Factor[2] (mm)
C1	135.2	5.18	6.40	4.49	0.2921	346.9	0.37846
C2	133.5	4.64	6.50	3.16	0.37338	272.3	0.48768
C3	129.7	3.86	8.00	3.25	0.29972	337.6	0.4318

1- Paste/Air Ratio values fall within the specifications recommended in ACI 201 and Appendix X1 of ASTM C457/C457M.
2- Void Frequency, Specific Surface, and Void Spacing Factor values do not fall within the recommended ranges in ACI 201 and Appendix X1 of ASTM C457/C457M. ASTM C457 Procedure B.

3.1. Petrographic Methodology

All three cores were examined visually and stereomicroscopically following ASTM C856. Air void system parameters were determined using ASTM C457, Procedure B (Modified Point Count). Portions of the cement paste from the samples were also analyzed under polarized light microscopy with refractive index oils to detect the presence of ground granulated blast-furnace slag (GGBFS). Photographs of the cores were taken at three stages including: as received in the lab, after lapping and following the application of phenolphthalein stain. The core images are included in Figures 2 to 9, along with photomicrographs of thin sections. Volumetric concrete proportions and air void system parameters are summarized in Tables 1 and 2, respectively.

Thin sections, approximately 25 microns thick, were prepared from each core to assess carbonation, the depth of deterioration, micro-fracturing, cement hydration, and the presence and extent of deleterious chemical reactions. Blue-dyed epoxy was used during thin section preparation to enhance the visibility of microstructural features

3.2. General Core Characteristics

The examined cores exhibited similar material characteristics. The concrete contained a 19 mm maximum size crushed micritic limestone. The coarse aggregate was fresh, angular, and densely packed. The fine aggregate was a subrounded natural sand comprised mainly of quartz with subordinate chert and granite and lesser coarse fines (limestone). Distribution of the aggregate was generally even, with no segregation or preferred orientation in any of the cores.

a) b) c)

Figure 2 a) Core C1 as received, b) sawn surface after the application of phenolphthalein stain indicating no carbonation, and c) sawn and polished surface. Fractures noted in red.

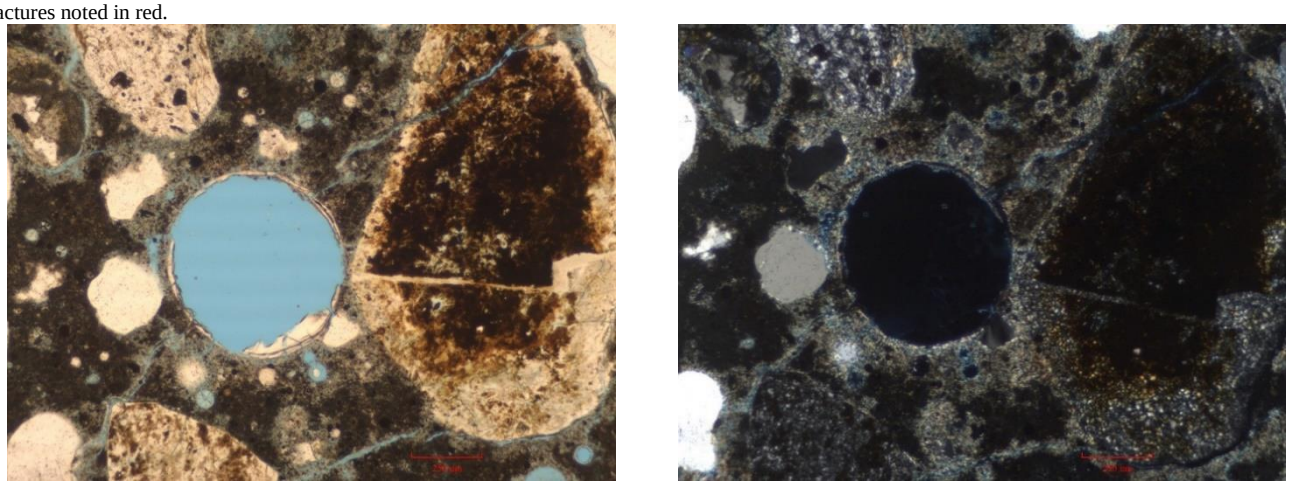

a) b)

Figure 3 a) Core C1 photomicrograph of alkali silica gel (ASR) lining a void with fractures through paste and aggregate. Plane polarized light. b) photomicrograph of alkali silica gel (ASR) lining a void with fractures through paste and aggregate. Cross polarized light.

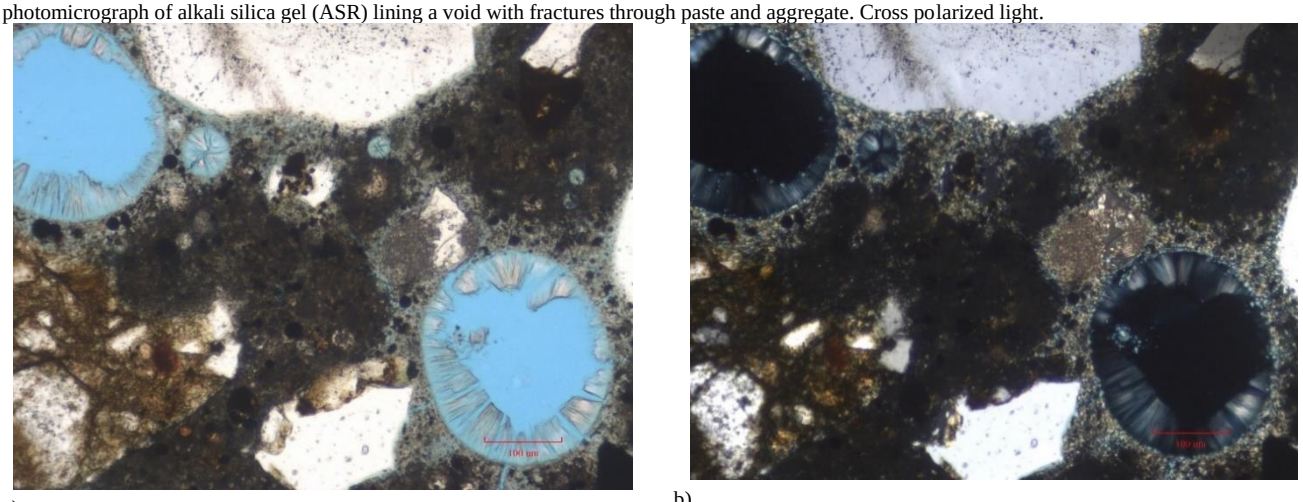

a) b)

Figure 4 a) Core C1 photomicrograph of ettringite lined/filled voids. Plane polarized light. b) photomicrograph of ettringite lined/filled voids. Cross polarized light.

Cementitious materials consisted of fairly to moderately well-hydrated Portland cement, with minor to moderate un-hydrated fly ash. The concrete was slightly to moderately air entrained. Void fillings were common, and most voids and fractures contained deposits of calcium hydroxide, calcium carbonate, ettringite, and varying degrees of ASR. Based on the application of phenolphthalein stain, the concrete was not carbonated.

Core C1 Summary of Analysis

The overall core was approximately 280 mm long by 95 mm in diameter. The core was received in the lab as intact, with a network of fine fractures throughout, illustrated in Figures 2 to 4. The exterior surface was sandy, slightly discolored, and exhibited slight chipping around the core circumference. The core was a full-depth core and terminated at an asphalt base. No steel reinforcement or wire mesh was observed.

Drilled surfaces exhibited moderate entrained air. Overall air content was 5.2%. Air distribution appeared moderately even throughout. No honeycombing nor coalescing voids were visibly apparent. Minor irregularly shaped voids were observed. The largest air void was approximately 6 mm in size. Void fillings were common, with most consisting of calcium hydroxide and calcium carbonate, as well as ettringite.

The matrix was hard and moderately dense. The matrix was greenish gray and uniform in color (Munsell color 5GY 5/1) when wet. Cementitious materials consisted of fairly to moderately hydrated Portland cement and fly ash. Slag cement was not present. Aggregate-matrix bonds were strong, with the concrete breaking predominantly through the coarse aggregate when struck by a hammer. However, micro-fracturing was common, and occurred both in the cement paste, and occasionally through limestone coarse aggregate particles. Calcium hydroxide was also observed in many of these fractures, as fillings/linings in voids, and along fracture surfaces. Moderate to abundant ettringite was frequently observed as both fracture and void fillings/linings. Alkali silica gel was observed in minor amounts as deposits in fractures. Based on the application of phenolphthalein stain, the concrete at this location was not carbonated.

Core C2 Summary of Analysis

The core was approximately 280 mm long by 95 mm in diameter and arrived in two pieces. The core was separated along an angular fracture at a depth of one to 50 mm. The

a) b) c)

Figure 5 a) Core C2 as received, b) sawn surface after the application of phenolphthalein stain indicating no carbonation. and c) sawn and polished surface. Fractures noted in red.

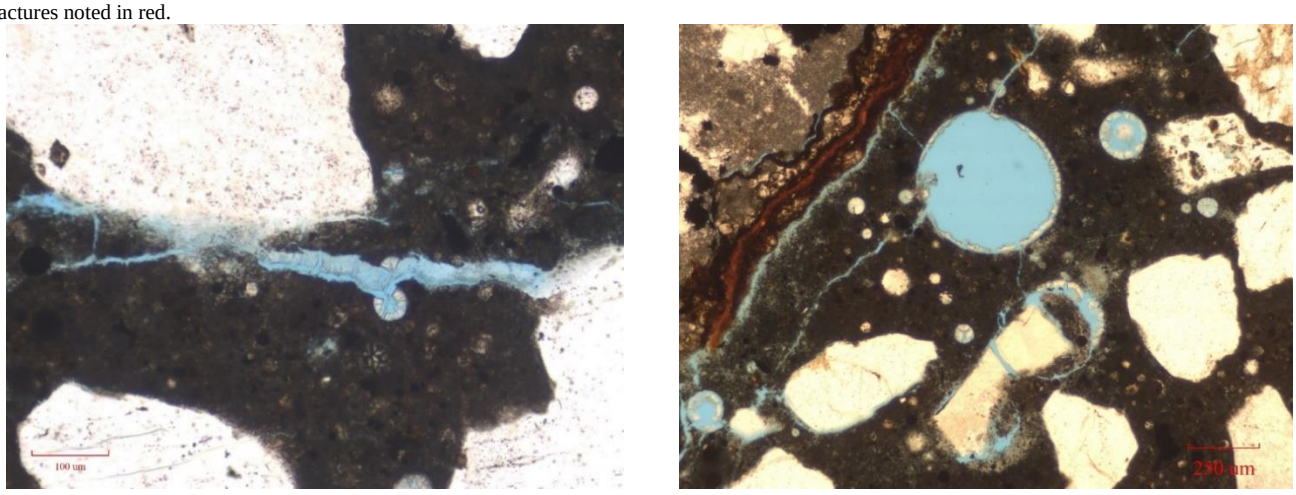

a) b)

Figure 6 a) Core C2 photomicrograph of ettringite filled fractures that have been displaced by continued widening of fractures. Plane polarized light. b) photomicrograph of fracturing and ettringite linings. Plane polarized light.

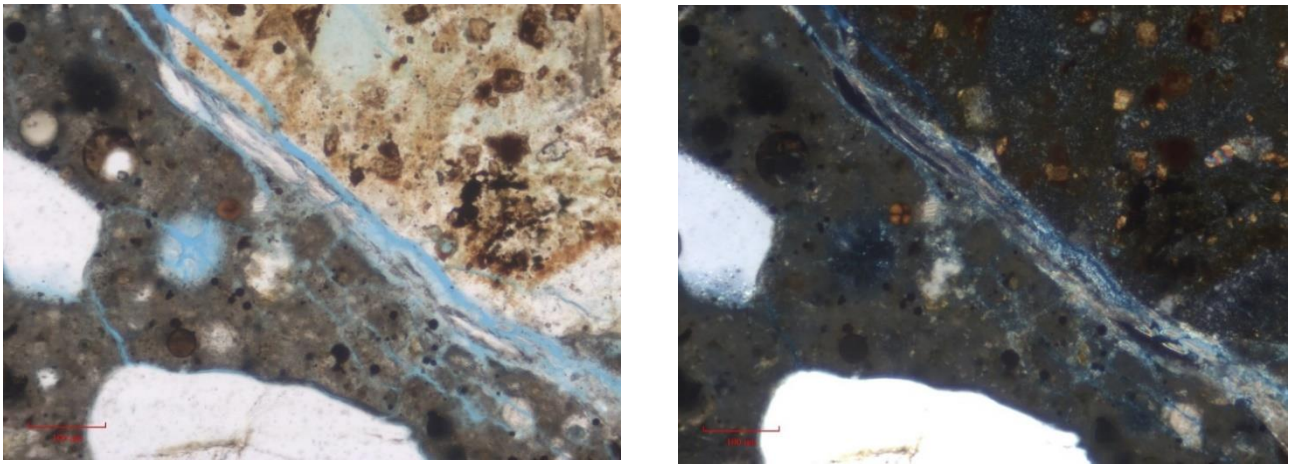

a) b)

Figure 7 a) Core C2 photomicrograph of alkali silica gel (ASR) filled fractures. Plane polarized light. b) photomicrograph of alkali silica gel (ASR) filled fractures. Cross polarized light.

top surface was sandy and exhibited a network of variably oriented fractures which extended to a depth of approximately 127 mm. The surface expression of these fractures was notably darker than the remainder of the surface. A network of fine, interior fractures was also observed throughout, illustrated in Figures 5 to 7. The core was full depth and terminated at an asphalt base with no steel reinforcement or wire mesh. Coarse and fine aggregates were similar to those observed in Core C1 in both size and composition.

Core C2 Summary of Analysis

The core was approximately 280 mm long by 95 mm in diameter and arrived in two pieces. The core was separated along an angular fracture at a depth of one to 50 mm. The top surface was sandy and exhibited a network of variably oriented fractures which extended to a depth of approximately 127 mm. The surface expression of these fractures was notably darker than the remainder of the surface. A network of fine, interior fractures was also observed throughout, illustrated in Figures 5 to 7. The core was full depth and terminated at an asphalt base with no steel reinforcement or wire mesh. Coarse and fine aggregates were similar to those observed in Core C1 in both size and composition

Drilled surfaces exhibited minor amounts of entrained air. Total air content was 4.6%. More than half of the air (2.4%) was entrapped air. Air distribution appeared moderately even throughout, and no honeycombing nor coalescing voids were visibly apparent. Minor irregularly shaped voids were observed. The largest air void was a “bug hole” approximately 22 mm in size. Void fillings were common, with most consisting of calcium hydroxide and calcium carbonate, as well as ettringite.

The matrix was hard and moderately dense. The matrix was dark greenish gray (Munsell color 10Y 4/1) and uniform in color when wet. Cementitious materials consisted of moderately hydrated Portland cement and minor fly ash. Slag cement was not apparent. Aggregate-matrix bonds were strong, with the concrete breaking predominantly through the coarse aggregate when struck by a hammer. Calcium hydroxide was observed in only minor quantities in the matrix and along matrix/aggregate interfaces. Surface micro-fracturing was not significant and randomly oriented. Discontinuous micro-fracturing was observed throughout the interior. Trace alkali-silica gel was observed as fillings/linings in some interior microfracture margins. Moderate to significant ettringite was observed as void fillings and linings. Based on the application of phenolphthalein stain, the concrete at this location was not carbonated

Core C3 Summary of Analysis

The core was approximately 260 mm long by 95 mm in diameter. The core was received intact, with no macroscopic fractures, illustrated in Figures 8 and 9. The top surface exhibited some wear and was sandy with minor exposed coarse aggregate. The core appeared to have been broken off at the bottom. No steel reinforcement or wire mesh was observed. Aggregate materials appeared to be similar to those in the previous two cores.

Drilled surfaces exhibited minor amounts of air. Total air content was 3.9%. More than half of the air (2.3%) was entrapped air. Air distribution appeared moderately even throughout, and no honeycombing nor coalescing voids were visibly apparent. Minor irregularly shaped voids were observed. The largest air void was approximately 6 mm in size. Void fillings were common, with most consisting of

calcium hydroxide and calcium carbonate, as well as ettringite.

The matrix was hard and moderately dense. The matrix was greenish gray in color (Munsell color 10Y 5/1) and uniform in color when wet. Cementitious materials were similar to those in the previous samples. Aggregate matrix bonds were moderate, with the concrete breaking predominantly, though not entirely, through the coarse aggregate when struck by a hammer. Micro-fractures were abundant, and many of the fractures contained calcium hydroxide and/or calcium carbonate. The micro-fractures appeared to be roughly oriented at 45 degrees to the core axis. Calcium hydroxide was also observed in minor quantities in the matrix and along matrix/aggregate interfaces. Based on the application of phenolphthalein stain, the concrete at this location was not carbonated.

4. Findings and Conclusions

A forensic investigation was conducted to evaluate the causes of deterioration in the concrete apron in a case study located in Nashville, Tennessee. The investigation involved detailed engineering observations, pavement condition surveys, and petrographic examinations of extracted concrete cores. The primary objective of this study was to assess the nature and extent of the distresses observed in the concrete apron and to provide recommendations for appropriate rehabilitation measures. The key findings and conclusions from the investigation are summarized as follows:

- The concrete represented by the examined cores exhibited similar composition and material characteristics. The concrete was generally well-proportioned, well-mixed, and well-consolidated, with a maximum coarse aggregate size of 19 mm consisting of crushed micritic limestone and fine aggregate composed primarily of natural sand. Cementitious materials included moderately hydrated Portland cement with minor quantities of unhydrated fly ash.

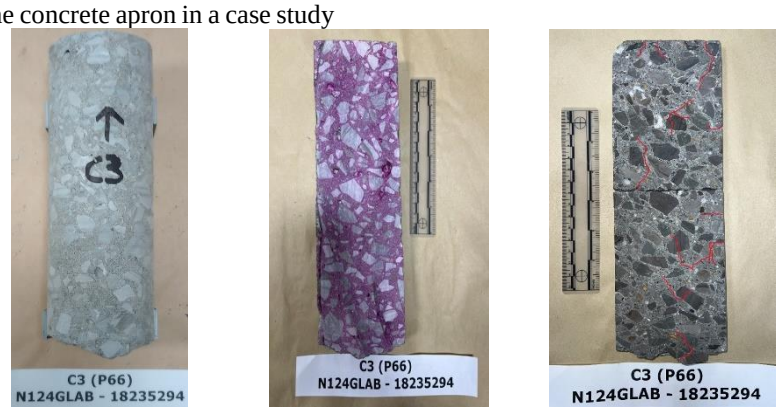

a) b) c)

Figure 8 a) Core C3 as received, b) sawn surface after the application of phenolphthalein stain indicating no carbonation, and c) sawn and polished surface. Fractures noted in red.

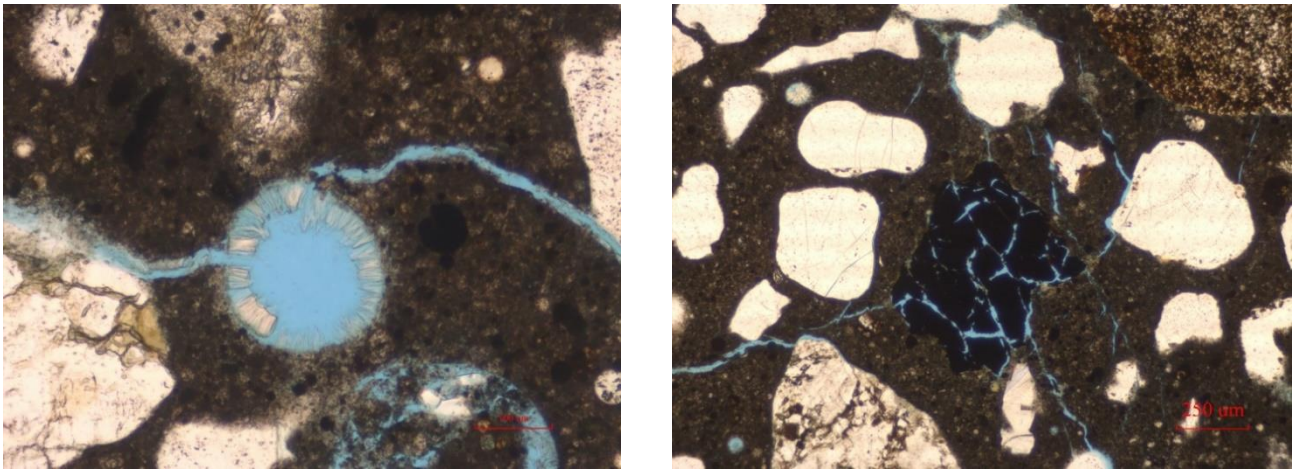

a) b)

Figure 9 a) Core C3 photomicrograph of ettringite lined voids and nearby fracture. Plane polarized light. b) photomicrograph of network of interior fracturing. Plane polarized light.

No slag cement was identified in the concrete matrix. The measured total air contents ranged from 3.9% to 5.2%, with the majority of the air in cores C2 and C3 consisting of entrapped air rather than entrained air. Air void spacing factors exceeded the ACI recommended maximum value of 0.2032 mm for optimal freeze-thaw durability. The distribution of air voids was generally uniform, with no evidence of honeycombing or coalescing voids.

- The petrographic analysis identified moderate to abundant ettringite, calcium hydroxide, and alkali-silica gel (ASR) in varying degrees within the concrete matrix. These materials were commonly observed as void fillings and along fracture surfaces. Calcium hydroxide was also frequently present along aggregate-matrix boundaries, suggesting ongoing chemical reactions and possible microstructural weakening. While evidence of ASR and secondary ettringite formation was observed, their presence was primarily confined to voids and fractures, indicating that they were not the dominant cause of the observed deterioration. The high air void spacing factors, which exceeded the ACI recommended limits, indicate that the concrete is susceptible to freeze-thaw damage. However, the fracture patterns observed in Core C2, including angular fractures and interior micro-fracturing, were not typical of distress caused solely by saturated freezing and thawing, suggesting that other mechanisms may also be contributing to the observed deterioration.
- The application of phenolphthalein stain to the core surfaces confirmed that the concrete was not carbonated. The absence of carbonation suggests that the chemical stability of the concrete matrix has not been compromised by carbon dioxide infiltration. The combination of distress patterns, the presence of ettringite and ASR, and the high air void spacing factors suggest that the observed deterioration is likely the result of multiple interacting mechanisms. Freeze-thaw damage due to inadequate air entrainment appears to be a primary contributing factor, with secondary contributions from possible sulfate attack (secondary ettringite formation) and ASR-related microstructural damage. However, the extent of ASR and sulfate attack appears to be limited and does not fully account for the observed distress patterns.
- Based on the findings, targeted repair strategies should address both the freeze-thaw susceptibility and the underlying chemical reactions within the concrete matrix. Improving air entrainment and implementing protective surface treatments may enhance the concrete's resistance to freeze-thaw cycles. Further evaluation of the sulfate and ASR activity, including long-term monitoring and potential mitigation measures, such as treating the surface with a solution of lithium nitrate, is also recommended to prevent future deterioration (Thomas et al, 2007). However, current studies have indicated limitations on the use of lithium nitrate treatment. Very little lithium penetrates below 25 to 50 mm unless the concrete is heavily cracked, and its ability to suppress ASR expansion is questionable Before treating a structure with lithium-based compounds it should be determined that the main cause is ASR, as the lithium treatment is unlikely to cure deterioration related to freeze-thaw damage, corrosion of embedded steel or even alkali-carbonate reaction. Further, there remains the potential for continued expansion and damage due to ASR, and the treatment will not "repair" any damage that has already occurred.
- In conclusion, the observed deterioration in the concrete apron is likely the result of a combination of inadequate freeze-thaw resistance, localized ASR, and possible sulfate attack. The prolific observation of D-cracking (i.e., cracking resulting from freeze-thaw) within the concrete apron is of significant concern as D-cracking is a terminal condition. Once it starts there's no known cure. D-cracking typically begins at the bottom of the concrete slab due to the natural accumulation of water under pavements in the base and subbase layers. The aggregate may eventually become saturated and crack from cycles of freezing and thawing and the cracking progresses upward to the surface of the slab where expansion, scaling and crumbling of the concrete surface occurs. The only way to prevent D-cracking is to avoid using coarse aggregates susceptible to freezing and thawing deterioration.

Acknowledgments

The authors would like to acknowledge the petrographers in the rock and soil mechanics laboratory facility in the Terracon Consultants, Inc. office in Cincinnati, Ohio for their help in providing the data in this research. The opinions, findings, and conclusions presented herein are those of the authors and do not necessarily reflect any sponsors.

Conflict of interest

The authors declare that they have no conflict of interest.

References

[1] ASTM International. "Standard Practice for Petrographic Examination of Hardened Concrete." ASTM C856-22 (2022).
[2] Fournier, B. and M. A. Bérubé. "Alkali-aggregate reaction in concrete: a review of basic concepts and engineering implications." Canadian Journal of Civil Engineering 27.2 (2000): 167–191.
[3] Grattan-Bellew, P. E. "Microstructural investigation of deteriorated concrete." Cement and Concrete Composites 17.1 (1995): 23–32.
[4] Abu-Farsakh, M., H. Alimohammadi, and L. N. Mohammad. "Finite Element Analysis to Evaluate the Benefits of Geosynthetic Reinforcement in Flexible Pavements Over Weak Subgrade for Low-Volume Traffic Roads." Transportation Research Board Conference 99th Annual Meeting (2020). https://annualmeeting.mytrb.org/OnlineProgramArchive/Details/12333
[5] Alimohammadi, H. and B. Izadi Babokani. "Finite element electrodynamics modeling of a layered piezoelectric composite shell with different materials by using numerical software." ISSS Journal of Micro and Smart Systems (2020). https://doi.org/10.1007/s41683-020-00052-3
[6] Poole, A. B. "Introduction to alkali-aggregate reaction in concrete." Proceedings of the International Conference on Alkali-Aggregate Reaction (1991): 1–19.
[7] Alimohammadi, H. "A framework for evaluation of existing pavement conditions and selection of feasible maintenance/rehabilitation alternatives; a case study in some routes of Livingston Parish in the state of Louisiana." SN Applied Sciences 2.2 (2020): 289. https://doi.org/10.1007/s42452-020-1999-6
[8] Zheng, G., H. Alimohammadi, J. Zheng, and V. R. Schaefer. "Effectiveness of Geosynthetics in the Construction of Roadways: A Full-Scale Field Studies Review." International Foundations Congress and Equipment Expo 2021 (2021): 223–232. https://doi.org/10.1061/9780784483411.022
[9] Sanchez, L. F. M., B. Fournier, and M. Jolin. "Evaluation of damage in concrete affected by ASR: A comparison of damage rating index and residual expansion tests." Construction and Building Materials 157 (2017): 139–151.
[10] Alimohammadi, H., V. R. Schaefer, J. Zheng, and H. Li. "Performance evaluation of geosynthetic reinforced flexible pavement: a review of full-scale field studies." International Journal of Pavement Research and Technology (2020). https://doi.org/10.1007/s42947-020-0019-y
[11] Alimohammadi, H., V. Schaefer, J. Ashlock, A. Buss, C. Rutherford, and B. Li. "Effectiveness of geogrids in roadway construction; determine a granular equivalent (G.E.) factor."
[12] Shehata, M. H. and M. D. A. Thomas. "The effect of fly ash composition on the expansion of concrete due to alkali–silica reaction." Cement and Concrete Research 30.7 (2000): 1063–1072.
[13] Alimohammadi, H., J. Zheng, A. Buss, V. R. Schaefer, C. Williams, and G. Zheng. "Field and simulated rutting behavior of hot mix and warm mix asphalt overlays." Construction and Building Materials 265 (2020): 120366. https://doi.org/10.1016/j.conbuildmat.2020.120366
[14] Kalhor, K., R. Ghasemizadeh, L. Rajic, and A. Alshawabkeh. "Assessment of groundwater quality and remediation in karst aquifers: A review." Groundwater for Sustainable Development 8 (2019): 104–121. https://doi.org/10.1016/j.gsd.2018.10.004
[15] Alimohammadi, H. and J. Tahat. "A case study experimental pile load testing (PLT) for evaluation of driven pile behaviors." Arabian Journal of Geosciences 15.9 (2022): 1–11. https://doi.org/10.1007/s12517-022-10176-5
[16] Alimohammadi, H. and J. Tahat. "A Case Study Pile Load Testing (PLT) to Evaluate Driven Pile Behaviors." Indian Geotechnical Journal 52 (2022): 959–968. https://doi.org/10.1007/s40098-022-00613-3
[17] Stark, D. "The moisture condition of field concrete exhibiting alkali-silica reactivity." Cement, Concrete, and Aggregates 13.1 (1991): 81–89.
[18] Alimohammadi, H., M. Amirmojahedi, and J. N. Tahat. "A Case History of Application of Deep Compaction Method with Comparison to Different Ground Improvement Techniques." Transportation Infrastructure Geotechnology (2022): 1–26. https://doi.org/10.1007/s40515-022-00229-3
[19] Satvati, S., H. Alimohammadi, M. A. Rowshanzamir, and S. M. Hejazi. "Evaluation the Effects of Geosynthetic Reinforcement on Bearing Capacity of Shallow Foundations in Soil Slopes." 101st Transportation Research Board Annual Meeting (2022). https://annualmeeting.mytrb.org/OnlineProgram/Details/17240
[20] Alimohammadi, H., V. R. Schaefer, J. Zheng, C. T. Jahren, G. Zheng, and D. White. "Effectiveness of Geotextiles/Geogrids in Roadway Construction; Determine a Granular Equivalent (GE) Factor." Minnesota Department of Transportation (2021). https://www.dot.state.mn.us/research/reports/2021/202126.pdf
[21] Alimohammadi, H., V. Schaefer, J. Zheng, D. J. White, and G. Zheng. "A State-of-the-art Large-scale Laboratory Approach to Evaluating the Effectiveness of Geogrid Reinforcement in Flexible Pavements." Geosynthetics Conference 2021 (2021). https://osf.io/2d4gk/
[22] Alimohammadi, H., A. Buss, V. R. Schaefer, J. Zheng, and G. Zheng. "Finite element viscoelastic simulations of rutting behavior of hot mix and warm mix asphalt overlay on flexible pavements." International Journal of Pavement Research and Technology (2020). https://doi.org/10.1007/s42947-020-0057-5
[23] Alimohammadi, H., J. Zheng, A. Buss, V. R. Schaefer, and G. Zheng. "Rutting Performance Evaluation of Hot Mix Asphalt and Warm Mix Asphalt Mixtures by Using Dynamic Modulus, Hamburg Wheel Tracking Tests, and Viscoelastic Finite Element Simulations." International Conference on Transportation and Development 2020 (2020): 83–94. https://doi.org/10.1061/9780784483183.009
[24] Zheng, J., H. He, and H. Alimohammadi. "Three-dimensional Wadell roundness for particle angularity characterization of granular soils." Acta Geotechnica 9 (2020). https://doi.org/10.1007/s11440-020-01004-9
[25] Alimohammadi, H., K. Yashmi Dastjerdi, and M. Lotfollahi Yaghin. "The study of progressive collapse in dual systems." Civil and

Environmental Engineering 16 (2020). https://doi.org/10.2478/cee-2020-0009

[26] Alimohammadi, H., J. Zheng, A. Buss, V. Schaefer, C. Williams, and G. Zheng. "Performance Evaluation of Hot Mix and Warm Mix Asphalt Overlay Layers Based on Field Measurements and Finite Element Viscoelastic Simulations." Transportation Research Board Conference 99th Annual Meeting (2020). https://annualmeeting.mytrb.org/OnlineProgramArchive/Details/13743

[27] Alimohammadi, H., A. Hesaminejad, and M. Lotfollahi Yaghin. "Effects of different parameters on inelastic buckling behavior of composite concrete-filled steel tubes." International Research Journal of Engineering and Technology 6.12 (2019). https://www.researchgate.net/publication/337856971_Effects_of_different_parameters_on_inelastic_buckling_behavior_of_composite_concrete-filled_steel_tubes

[28] Stark, D. and D. Gress. "Effects of alkali-silica reaction on concrete pavements." Transportation Research Record 1448 (1994): 54–61.

[29] Alimohammadi, H., M. D. Esfahani, and M. L. Yaghin. "Effects of openings on the seismic behavior and performance level of concrete shear walls." International Journal of Engineering and Applied Sciences (2019). https://www.researchgate.net/publication/337596926_Effects_of_openings_on_the_seismic_behavior_and_performance_level_of_concrete_shear_walls

[30] Alimohammadi, H. "Finite element analysis of a Piezoelectric layered plate with different materials." International Journal of Engineering and Applied Sciences 6.7 (2019). https://doi.org/10.31873/IJEAS.6.8.2019.09

[31] Thomas, M. D. A., B. Fournier, and K. J. Folliard. "Report on the diagnosis, prognosis, and mitigation of alkali-silica reaction (ASR) in transportation structures." FHWA Report No. FHWA-HIF-13-019 (2013).

[32] Alimohammadi, H. and M. Lotfollahi Yaghin. "Study on the Effect of the Concentric Brace and Lightweight Shear Steel Wall on Seismic Behavior of Lightweight Steel Structures." International Research Journal of Engineering and Technology 6.8 (2019): 1358–1362. https://www.researchgate.net/publication/336846191_Study_on_the_Effect_of_the_Concentric_Brace_and_Lightweight_Shear_Steel_Wall_on_Seismic_Behavior_of_Lightweight_Steel_Structures

[33] Alimohammadi, H. and M. Abu-Farsakh. "Finite Element Parametric Study on Rutting Performance of Geosynthetic Reinforced Flexible Pavements." Transportation Research Board 98th Annual Meeting (2019). https://trid.trb.org/view/1572248

[34] Alimohammadi, H. and A. Memon. "A Case Study of Mechanically Stabilized Earth (MSE) Retaining Wall Failure in the State of Tennessee; Recommendations for Future Design and Constructions." OSF Preprints (2023). https://doi.org/10.31219/osf.io/uy76r

[35] Alimohammadi, H., V. R. Schaefer, J. Zheng, and D. White. "A full-scale field approach for evaluating the geogrid reinforcement effectiveness in flexible pavement." 22nd International Conference on Soil Mechanics and Geotechnical Engineering (2022).

[36] Alimohammadi, H. and J. Tahat. "A State-of-The-Art Evaluation of Driven Pile Behaviors Using Pile Load Testing (PLT)." 101st Transportation Research Board Annual Meeting (2022). https://annualmeeting.mytrb.org/OnlineProgram/Details/17332

[37] Alimohammadi, H. "Effectiveness of Geogrids in Roadway Construction: Determine a Granular Equivalent (G.E.) Factor." Iowa State University (2021). https://www.proquest.com/docview/2576937127

[38] Alimohammadi, H. "Rutting Behavior of Laboratory, Field, and Finite Element Simulated Hot Mix and Warm Mix Asphalt Overlays." Iowa State University (2021).

[39] Thomas, M. D. A., B. Fournier, K. J. Folliard, J. H. Ideker, and Y. Resendez. "The Use of Lithium to Prevent or Mitigate Alkali-Silica Reaction in Concrete Pavements and Structures." FHWA Report No. FHWA-HRT-06-113 (2007).

[40] Alimohammadi, H. and M. Abu-Farsakh. "Evaluating Geosynthetic Reinforcement Benefits of Flexible Pavement." 8th Annual Graduate Student Research Conference (2019).

[41] Alimohammadi, H. and A. Memon. "Failure Analysis and Recommendations For Improving Mechanically Stabilized Earth (MSE) Retaining Wall Design and Construction: A Case Study from Tennessee, USA." Transportation Research Board 103rd Annual Meeting (2024).

[42] Alimohammadi, H. and A. Memon. "A Case Study of Failure Analysis of an MSE Retaining Wall in Tennessee: Lessons Learned and Recommendations for Reconstruction." OSF Preprints (2023). https://doi.org/10.31219/osf.io/nf95e

[43] Alimohammadi, H. and A. Memon. "Forensic Investigation of Slope Stability Issues and Design Practices: A Case Study in Nashville, Tennessee." OSF Preprints (2023). https://doi.org/10.31219/osf.io/9yx82

[44] Alimohammadi, H. and J. Tahat. "Evaluation of Driven Pile Using Pile Load Testing: A Case Study in the State of Ohio." Geo-Congress 2024 (2024).

[45] Alimohammadi, H. and J. Tahat. "Evaluating Driven Pile Behaviors Through Case Study Experimental Pile Load Testing (PLT)." 48th Annual Conference on Deep Foundations (2023).

[46] Satvati, S., H. Alimohammadi, M. Rowshanzamir, and S. M. Hejazi. "Bearing Capacity of Shallow Footings Reinforced with Braid and Geogrid adjacent to Soil Slope." International Journal of Geosynthetics and Ground Engineering 6.41 (2020). https://doi.org/10.1007/s40891-020-00226-x

[47] Alimohammadi, H., J. Zheng, A. Buss, V. R. Schaefer, and G. Zheng. "Evaluating the Rutting Performance of Hot Mix Asphalt and Warm Mix Asphalt Mixtures by Using Viscoelastic Finite Element Simulations." International Conference on Transportation and Development 2020 (2020). https://doi.org/10.1061/9780784483183.009

[48] Swamy, R. N. "The alkali-silica reaction in concrete." Spon Press (2002).

[49] Alimohammadi, H., J. Zheng, V. Schaefer, J. Siekmeier, and R. Velasqueze. "Evaluation of Geogrid Reinforcement of Flexible Pavement Performance: A Review of Large-Scale Laboratory Studies." Transportation Geotechnics (2020). https://doi.org/10.1016/j.trgeo.2020.100471

[50] Alimohammadi, H. and B. Izadi Babokani. "Finite element electrodynamics modeling of a layered piezoelectric composite shell with different materials by using numerical software." ISSS Journal of Micro and Smart Systems (2020). https://doi.org/10.1007/s41683-020-00052-3

[51] Alimohammadi, H. and M. D. Esfahani. "Investigating the Opening Effect of Constant Cross-Section and Various Forms of Seismic Behavior and Performance levels in Concrete Shear Walls." First international conference on civil engineering architecture and stable urban development (2015).

[52] Alimohammadi, H. and M. Lotfollahi Yaghin. "Evaluation of seismic properties of light weight concentric brace on seismic behavior of light weight steel structures." National Conference in applied civil engineering and new advances (2014).

[53] Alimohammadi, H. and M. Lotfollahi Yaghin. "Evaluation of seismic properties of lightweight steel frames coated with lightweight steel shear wall." First international conference on urban

development based on new technologies and 4th national conference on urban development (2014).

[54] Wang, X., J. Lai, S. He, and Y. Wang. "Karst geology and mitigation measures for hazards during metro system construction in Wuhan, China." Natural Hazards 103 (2020): 2905–2927. https://doi.org/10.1007/s11069-020-04108-3

[55] Song, K-I., G-C. Cho, and S-B. Chang. "Identification, remediation, and analysis of karst sinkholes in the longest railroad tunnel in South Korea." Engineering Geology 135–136 (2012): 92–105. https://doi.org/10.1016/j.enggeo.2012.02.018

[56] Gracia, A., F. J. Torrijo, J. Garzón-Roca, M. Pérez-Picallo, and O. Alonso-Pandavenes. "Identification and Mitigation of Subsidence and Collapse Hazards in Karstic Areas: A Case Study in Alcalá de Ebro (Spain)." Applied Sciences 13.9 (2023): 5687. https://doi.org/10.3390/app13095687

[57] Goldscheider, N. "A holistic approach to groundwater protection and ecosystem services in karst terrains." Carbonates and Evaporites 34 (2019): 1241–1249. https://doi.org/10.1007/s13146-019-00492-5

[58] Alimohammadi, H. "Shallow Foundations and Deep Foundations; Drilled Piers, Aggregate Piers and Stone Columns; Design Recommendations, Construction Considerations, and Performance." Journal of Civil Engineering Researchers 6.3 (2024): 18–28. https://doi.org/10.61186/JCER.6.3.18

[59] Alimohammadi, H. and A. Memon. "Comprehensive Sinkhole Mitigation: A Case Study and Application of Compaction Grouting in Karstic Environments in the State of Tennessee, USA." Journal of Civil Engineering Researchers 6.2 (2024): 1–16. https://doi.org/10.61186/JCER.6.2.1

[60] Alimohammadi, H. and A. Memon. "Mitigation of A Sinkhole in Nashville, Tennessee: A Case Study with Compaction Grouting Approach." OSF Preprints (2024). https://osf.io/preprints/osf/63nyv_v1

[61] Alimohammadi, H. and A. Memon. "Failure Analysis and Recommendations For Improving Mechanically Stabilized Earth (MSE) Retaining Wall Design and Construction: A Case Study from Tennessee, USA." Transportation Research Board 103rd Annual Meeting (2024).

[62] Alimohammadi, Hossein and Behrooz Izadi Babokani. "Finite element electrodynamics modeling of a layered piezoelectric composite shell with different materials by using numerical software." ISSS Journal of Micro and Smart Systems 9.1 (2020): 79–88. https://doi.org/10.1007/s41683-020-00052-3